






RESEARCH ARTICLE | NOVEMBER 10 2023

Comparing magnetic pushing to underwater explosions for flyer acceleration

D. Maler ; G. Liziakin ; O. Belozerov ; S. Efimov ; D. Rakhmilevich; K. Cohen ; Ya. E. Krasik 

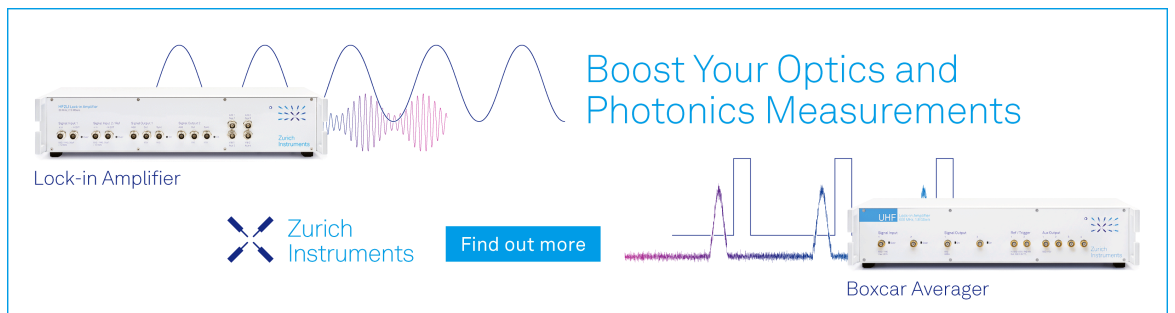


J. Appl. Phys. 134, 185902 (2023)


<https://doi.org/10.1063/5.0176294>



Boost Your Optics and Photonics Measurements



Lock-in Amplifier



Zurich Instruments

Find out more

Boxcar Averager

Comparing magnetic pushing to underwater explosions for flyer acceleration

Cite as: J. Appl. Phys. 134, 185902 (2023); doi: 10.1063/5.0176294

Submitted: 12 September 2023 · Accepted: 21 October 2023 ·

Published Online: 10 November 2023



D. Maler,^{a)} G. Liziakin, O. Belozarov, S. Efimov, D. Rakhmievich, K. Cohen, and Ya. E. Krasik

AFFILIATIONS

Department of Physics, Technion—Israel Institute of Technology, Haifa 3200003, Israel

^{a)}Author to whom correspondence should be addressed: daniel.maler@campus.technion.ac.il

ABSTRACT

We present results exploring various methods of aluminum flyer acceleration. One method uses the shock wave generated by underwater electrical explosions of thin foils supplied by a pulse generator with stored energy of ~ 4.7 kJ. Utilizing the shock created by an exploding foil, a maximal free flyer velocity of ~ 2000 m/s is obtained. This acceleration method is compared to results exploiting only magnetic pushing to accelerate flyers using a common strip-line configuration, resulting in much lower velocities of ~ 300 m/s. We also present a modified strip-line configuration, for which a significant increase in the flyer velocity to ~ 1200 m/s is measured. Finally, a hybrid strip configuration, incorporating both the effects of magnetic pushing and acceleration by exploding foil and its subsequent shock wave, results in ~ 1400 m/s flyer velocity. These experimental results are analyzed by numerical simulations and analytical modeling of the conservation equations of mass and momentum.

© 2023 Author(s). All article content, except where otherwise noted, is licensed under a Creative Commons Attribution (CC BY) license (<http://creativecommons.org/licenses/by/4.0/>). <https://doi.org/10.1063/5.0176294>

I. INTRODUCTION

When studying matter under extreme conditions, it is common practice to accelerate flyer plates to high velocities required in impact experiments. This technique is used to generate upon impact, strong shockwaves inside a material, allowing interpolation of the parameters of its equations of state (EOS) (pressure, density, and temperature) together with the Rankine–Hugoniot conservation equations.^{1–3} Acceleration of flyers to high velocities ($>10^3$ m/s) is performed by using explosives,⁴ gas guns,⁵ focused laser beams,^{6,7} magnetic field gradients,⁸ and underwater electrical explosions of wire arrays.^{9,10} The use of explosives and gas guns requires special safety measures while laser launched flyer plates are typically of sub-mm dimensions limited by the laser beam's focal spot size.

The acceleration of flyer plates (flyers) using strong magnetic field gradients utilizes the $J \times B$ force to exert high magnetic pressure on current carrying electrodes, yielding high velocities of the material. For this acceleration method, known as magnetic pushing,⁸ a strip-line configuration is utilized with two parallel electrodes in which current flows in opposite directions and a thin dielectric sheet between them. This design results in a very low-inductance load with the magnetic field confined inside the interelectrode gap. For high-current generators, such as the Z-machine,¹¹ this setup is

held in vacuum with a small (<1 mm) gap and current densities $>10^8$ A/cm² so that explosive surface plasma is formed.¹² The plasma can destroy the dielectric sheet and shorten the gap between the electrodes resulting in current losses at the load.

Recently, an alternative approach for launching flyer plates by underwater electrical explosion of planar wire arrays using pulsed high-current generators was presented.^{9,10} Here, the flyer is placed above the exploding wire array, which is immersed in water, and is accelerated by the strong shock generated by the array and the subsequent waterflow behind the shock front. This method was demonstrated as being very efficient in converting the energy stored in the generator to the flyer kinetic energy (up to $\sim 20\%$). In addition, the measurement of material flow, strain rate, and shock velocity inside the flyer can be performed along Hugoniot curves.

For a wire array, the explosion of each wire is accompanied by the generation of a cylindrical strong shock. The overlap between adjacent shocks forms a planar shock at some distance from the array depending on the inter-wire spacing. In order to obtain a planar shock at a distance of <1 mm from the array, where shock pressure is maximal, the inter-wire spacing should be <0.5 mm. This requires increasing the number of wires (>60) and consequently decreasing the wire diameter ($<20 \mu\text{m}$) to keep an almost

17 April 2024 11:03:13

critically damped discharge for maximum energy density deposition rate into the wires.¹³

The use of thin metal foils in electrical explosions was demonstrated and studied in vacuum and air.^{14,15} In Ref. 15, the acceleration of various materials to high velocities by the explosions of aluminum foils has shown efficient energy transfer of up to ~25% into the kinetic energy of the flyer. Thus, a foil geometry can be advantageous for generating planar shocks at small distances from the exploding conductor.

In this work, we present a direct comparison of flyer acceleration by underwater electrical explosions in three configurations. First, we present a strip-line configuration with de-ionized water as the insulation medium between electrodes and perform flyer acceleration by magnetic pushing. In addition, a modification of this configuration is presented, resulting in a considerable increase in the magnetic field density. Second, we demonstrate that an underwater explosion of thin metal foils can be used to launch flyers floating on water to high velocities. Finally, we present a hybrid configuration, which utilizes both the effect of magnetic pushing and acceleration by the shock of an exploding foil in a strip-line configuration. Experimental results are then compared and analyzed by numerical simulations, recreating the experimental conditions.

II. EXPERIMENTAL SETUP, DIAGNOSTICS, AND RESULTS

All experiments were carried out on the high-current MAGEN¹⁶ pulse generator of 1.92 μF capacitance, operated at the same a charging voltage of 70 kV (stored energy of 4.7 kJ). Current and voltage waveforms, measured using a self-integrated Rogowski coil and a P6015A Tektronix voltage divider, were acquired by a

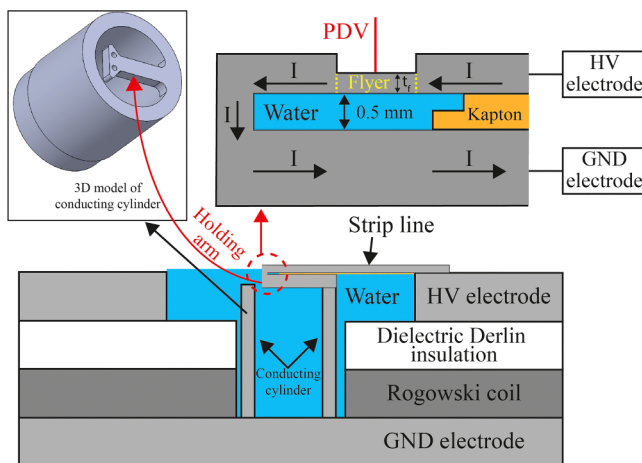


FIG. 1. Cross section of the experimental setup of the strip-line configuration. The upper diagram is an enhanced view of the dashed red circle. The 3D model depicts the conducting grounded (GND) cylinder and the holding arm on which the strip line is attached. Arrows marked by I denote the direction of the current flow.

Tektronix TDS 640A digitizing oscilloscope. In measurements with exploding foils, the resistive voltage was calculated as $V_{\text{res}} = V - L_l \left(\frac{dI}{dt}\right)$, where V is the measured voltage, L_l is the load inductance, and I is the measured current.

The surface velocity of accelerated flyers was obtained using a self-assembled photonic Doppler velocimetry^{9,17} (PDV). The main continuous wave (CW) laser beam ($\lambda_0 = 1550.12$ nm, 250 mW) reflected from the moving flyer is interfered with a reference CW laser (1550.132 nm, 0.5 mW) resulting in an initial heterodyne frequency of ~1.4 GHz for stationary flyer. The maximal power of the reflected beam was ~0.4 mW. The interfered signal was recorded using an Agilent Infiniium 54855A DSO digitizing oscilloscope (6 GHz, 20 Gs/s). The collimated main laser beam was directed toward the flyer using a fiber coupled lens with a focal length of ~50 mm, which also detected the reflected light. The fiber lens was mounted upon a 3D printed holder and positioned at a distance equal to the focal point directly above the flyer to maximize the power of the reflected signal. A spectrogram was extracted from the interfered signal to determine the flyer velocity's temporal evolution, which was calculated as $v = 0.5\Delta f\lambda_0$, where Δf is the change in the signal frequency. The error in velocity was estimated as $\delta v = \pm 30$ m/s. A B-dot signal was used to synchronize between the acquired waveforms of the discharge current and the signal registered from the PDV.

A. Strip-line configuration

The essential part of the strip-line configuration is seen in the magnified region depicted in Fig. 1. The strip line consists of two, 30 mm long and $W = 7$ mm wide, parallel rectangular aluminum plates of 2 mm (upper plate) and 5 mm (lower plate) thickness. The gap between the plates was set to $d = 0.5$ mm and filled with de-ionized water. A 0.4 mm-thick Kapton foil filled the gap at the input end of the strip line to avoid breakdown between the high voltage (HV) and grounded (GND) electrodes. Finally, a circular 7 mm diameter and $t_f = 1.5$ mm thick indentation was machined into the middle of the upper electrode. This thin circular region is the flyer toward which the PDV laser was directed (see Fig. 1).

Waveforms of the discharge current and voltage are shown in Fig. 2(a) and the flyer velocity's temporal evolution together with the discharge current on a longer timescale are shown in Fig. 2(b). The total inductance, including the inductance of the conducting cylinder and the strip line, was estimated as $L \sim 23$ nH from the initial rapid rise of the measured voltage. The current reached a maximal amplitude of $I_{\text{max}} \sim 460$ kA with a rise time of ~420 ns. Considering a strip-line inductance of $L_{\text{str}} = 4\pi \times 10^{-7} l(d/W) = 2.7$ nH, and an inductive voltage at the input of the strip line ≤ 3 kV, a corresponding average electric field of 60 kV/cm is realized. At maximal current, the magnetic pressure, assuming uniform linear current density distribution, can reach $P = 2\pi \times 10^{-7} (I_{\text{max}}/W)^2 \cong 2.7 \times 10^9$ Pa. The flyer velocity's temporal evolution exhibited multiple acceleration steps [see Fig. 2(b)], corresponding to the oscillating nature of the discharge current, quadratically proportional to the magnetic pressure. The initial rise of the flyer velocity was ~150 m/s within 450 ns (maximal acceleration of $\sim 3 \times 10^8$ m/s²), reaching a maximal velocity of ~300 m/s within ~4 μs . Additionally, these experiments show that water can be used as the insulator between the strip-line electrodes

17 April 2024 11:03:13

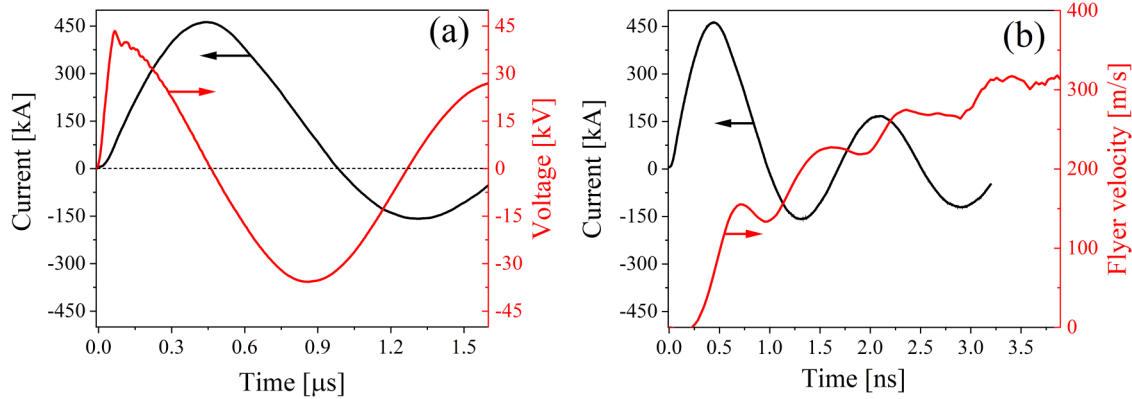


FIG. 2. Waveforms of the discharge current and voltage (a) and the temporal evolution of the flyer velocity synchronized with the waveform of the discharge current (b). Flyer holding arm as in Fig. 3 (left).

near the flyer with proper insulation elsewhere for electric fields not exceeding 100 kV/cm.

B. Modified strip-line configuration

The essential part of the experimental arrangement seen in Fig. 1 is held on a platform, which is a conducting arm attached to the ground as seen in Fig. 3 (left). The linear current distribution in the few mm wide strip line cannot be considered uniform because of the significantly larger current density at the edges

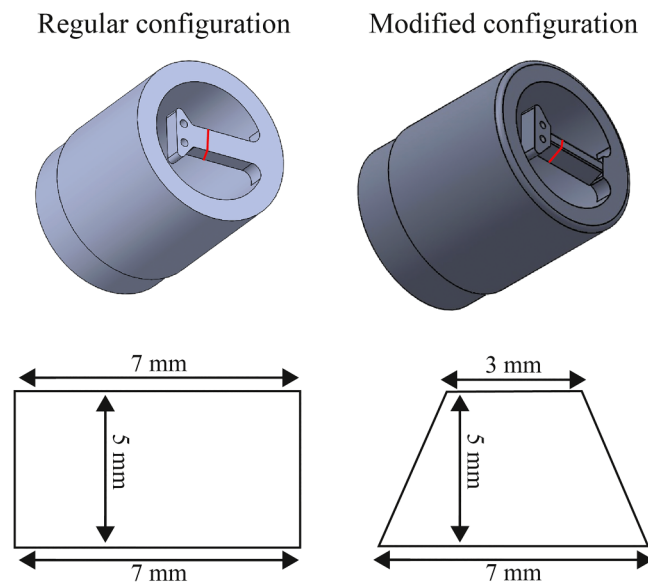


FIG. 3. 3D model of the conducting cylinder and holding arm for the strip-line configuration. Left image is the original design while the right image depicts the modified version. The red line denotes the position where below each model, the cross section is depicted.

where a very intense electric field is also present. In order to reduce this effect, a modified shape of the holding arm was designed [Fig. 3 (right)]. Here, the holding arm is machined to have a reduced cross section shaped as an isosceles trapezoid. This design, as it will be discussed below, results in a uniform linear current density distribution with a substantial increase in the magnetic field strength below the flyer.

The waveforms of the discharge current and voltage together with the flyer velocity's temporal evolution obtained in these experiments are presented in Figs. 4(a) and 4(b), respectively. The waveforms of the current and voltage are almost the same as those in Fig. 2(a) showing that the increase in the inductance of the strip line is insignificant compared to the total load inductance. However, due to the increase in the linear current density, the magnetic pressure increases up to $\sim 1.5 \times 10^{10}$ Pa which results in almost four times larger maximum flyer velocity [compare to Fig. 2(b)]. The first jump in velocity reached ~ 380 m/s within 330 ns (maximal acceleration of $\sim 10^9$ m/s²) with further increase up to ~ 1200 m/s within ~ 4 μs.

The above modification of the strip-line configuration led to the enhanced magnetic field in the gap between electrodes, resulting in higher flyer velocity. To verify this, simulations of the current density and magnetic fields, at the cross section perpendicular to the current flow, were performed using the COMSOL Multiphysics software. To recreate the experimental conditions, the peak current in the simulations was set to 450 kA with a frequency of 625 kHz. Both geometrical configurations described in Sec. II A (flat geometry) and above (trapezoid geometry) were simulated, with results presented in Fig. 5.

Figures 5(a) and 5(b) depict the distribution of the magnetic field in the gap between the strip-line electrodes for both configurations. Figures 5(c) and 5(d) depict the magnitude of the magnetic field in the inter-electrode gap at three different heights [see y axis in (e) and (f)]. We note that the distribution of the magnetic field in both configurations is uniform along the gap. Moreover, the reduction in the width of the lower electrode increases the magnetic field ~ 1.5 times from ~ 65 to ~ 96 T, resulting in over twice the

17 April 2024 11:03:13

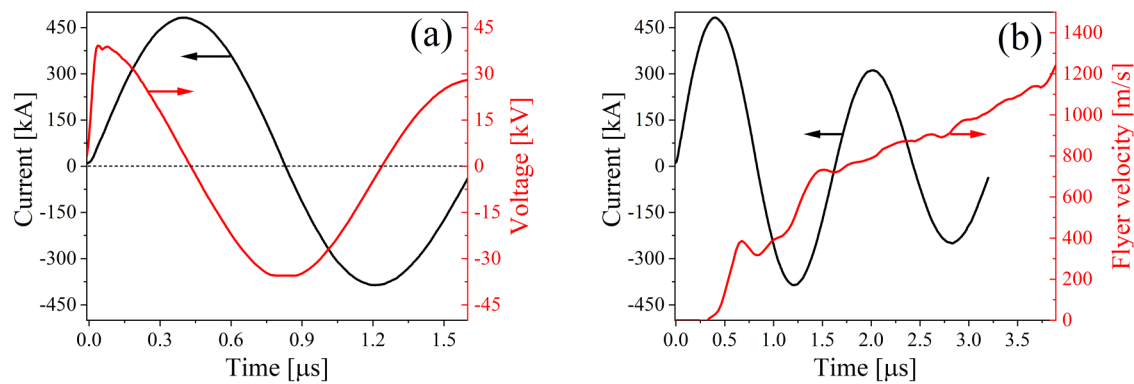


FIG. 4. Waveforms of the discharge current and voltage (a) and the temporal evolution of the flyer velocity synchronized with the waveform of the discharge current (b). Flyer holding arm as in Fig. 3 (right).

magnetic pressure. This is also visible in Figs. 5(e) and 5(f), where the distribution of the current density shifts from the edge of the electrodes in the flat geometry to being localized at the middle of the upper electrode, where the flyer is located.

C. Floating flyer configuration

In this set of experiments, we used the floating flyer configuration, which was similar to that studied in our earlier research,^{9,10} where flyers were accelerated by the underwater electrical explosion of a planar wire array. The flyer in this configuration is an aluminum disk, which is not part of the electrode as in previous configurations. To obtain a planar symmetric shock wave by wire array explosions with minimal time jitter between individual exploding wires,¹³ a large number (>60) of thin (tens of μm) wires separated by sub-mm distances is required. In the present experiments, the wire array is replaced by aluminum (Al) or copper (Cu) thin foils. The cross section of these foils was adjusted to produce an almost critically damped discharge with a current fall time less than the quarter period of an oscillatory underdamped discharge. The essential part of this experimental setup is presented in Fig. 6. A 1.5 mm-thick and 3 mm-diameter aluminum flyer disk is placed on a 0.2 mm-thick and 2.5 mm-diameter Perspex holder to float on the water at a fixed position at a distance of ~2 mm from the foil, which is submerged in water. The bottom part of the flyer is in contact with water while its upper surface with air and illuminated by the PDV laser.

The waveforms of the discharge current, resistive voltage, power, and deposited energy for Al foils are presented in Figs. 7(a) and 7(b) and for Cu foil explosions in Figs. 7(c) and 7(d). Both Al and Cu foils were 8 mm wide and 40 mm long. The foil thickness was 50 μm for Al and 35 μm for Cu. The total cathode holder and foil inductance was estimated as ~44 nH. An almost critically damped discharge current was obtained for both foils with current amplitudes of ~280 and ~300 kA and rise times of ~400 and ~430 ns for Al and Cu foils, respectively. A significantly smaller amplitude of the current, compared to the strip-line configuration experiments, is explained by the energy deposited into the foil,

inducing solid-liquid-vapor phase transitions resulting in significantly larger resistance of the exploding foils compared with the strip-line resistance. This decrease in current, combined with the increase in the gap to 2 mm, causes the effects of magnetic pushing to be negligible. The energy density deposition rate, calculated at full duration half maximum of the deposited power, was 2.27×10^5 and $1.05 \times 10^5 \frac{\text{MJ}}{\text{g s}}$, while the deposited energy density was ~21 and ~23 eV/atom for Al and Cu foils, respectively. These values of the energy density deposition rates and deposited energy density are similar to those obtained in our earlier research with planar wire array explosions.¹⁰

The temporal evolution of the flyer velocities, obtained in this set of experiments, is shown in Fig. 8. For both foils, a similar initial velocity jump of up to ~700 m/s is observed, the result of the interaction of the strong shock generated by the exploding foils with the flyer. This jump is followed by a velocity plateau, which represents the waterflow pushing the flyer. This velocity plateau can be qualitatively considered to be related to two competitive processes. In particular, as the flyer accelerates, its distance from the foil increases and the pressure of the waterflow decreases. However, the foil expansion compensates for this effect. After ~1.5 μs for Al foil and ~1.8 μs for Cu foil explosions, a second jump in velocity is observed, reaching ~1800 and 1100 m/s, respectively. The PDV signal contained much more interference for Al foil explosions than for Cu but the flyer velocity could still be reliably evaluated. We relate this second increase in velocity with the interaction of the expanding foil with the target. Indeed, the time delay in appearance of the second jump in velocity is ~2.7 μs relative to the maximum of the discharge current when fast expansion of the foil starts. Taking this time delay, relative to the maximal power and considering target displacement, one obtains an average foil expansion velocity of ~1000 m/s. To verify this assumption, additional experiments with the floating targets placed at 1 mm from the Al foil were performed results of which are presented in Fig. 8(c). One can see that due to the proximity of the flyer to the expanding Al foil, the second increase in velocity occurs earlier, ~0.9 μs relative to the time of the first jump in velocity. This strengthens our explanation for the second jump as being the result of foil-flyer

17 April 2024 11:03:13

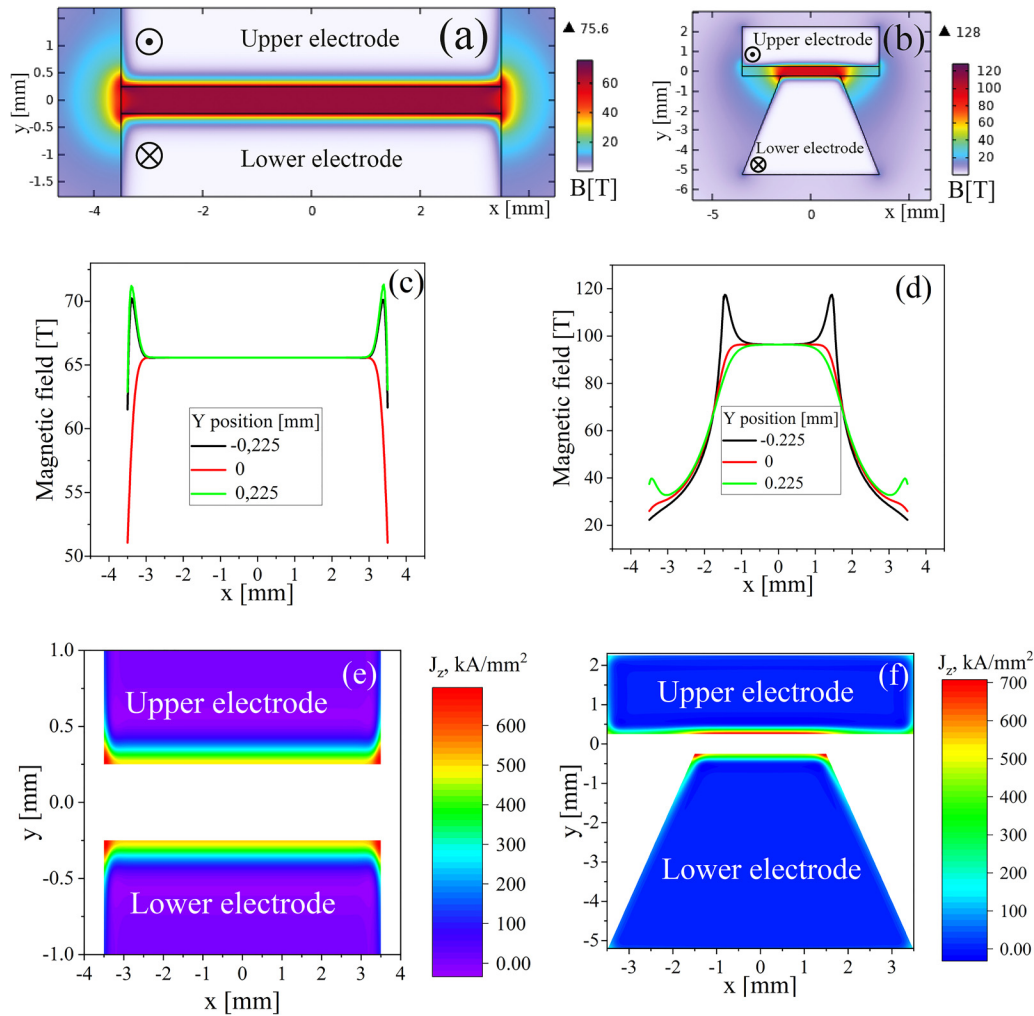


FIG. 5. Simulated magnetic field spatial distribution [(a) and (b)], magnetic field in the inter-electrode gap along x at various positions y [(c) and (d)], and the spatial distribution of the current density for the flat [(a), (c), and (e)] and trapezoid [(b), (d), and (f)] geometry, respectively. The circles in (a) and (b) mark the direction of current flow.

interaction. We also note that in this experiment, the second jump in velocity is higher, i.e., ~ 2000 m/s. Due to the fast rise in velocity, a shock might be created inside the target following the interaction with the exploded foil, inducing the rapid acceleration of the flyer material at the free boundary. Considering a ~ 2000 m/s free surface velocity, corresponding to ~ 1000 m/s material flow velocity, one obtains ~ 60 J kinetic energy of the flyer. To conclude, in these floating flyer experiments, significantly higher flyer velocities are achieved than with the strip-line configurations.

D. Hybrid configuration

Finally, we tested a hybrid configuration that incorporates both the low-inductive structure of the strip line, taking advantage of magnetic pushing, and the strong shock generation of the

exploding foil. In this configuration, the upper part of the strip line containing the circular flyer is similar to that described in Sec. II A. The lower electrode contains the exploding Al or Cu foils as in Sec. II C. The gap between the foil and the strip line was filled with a 1 mm-thick volume of de-ionized water separated from the lower surface of the strip line. Additionally, a ~ 0.3 mm-thick Kapton foil was glued to the upper strip line to avoid electrical breakdown initiated by the exploding foil (see Fig. 9). The gap between the foil and the strip line was ~ 1.3 mm, which is 2.6 times larger than in the case of the strip-line configurations described in Secs. II A and II B.

The waveforms of the discharge current, resistive voltage, power, and deposited energy for Al foil explosions are presented in Figs. 10(a) and 10(b). Similar waveforms for the Cu foil explosions are presented in Figs. 10(c) and 10(d). In both explosions, the

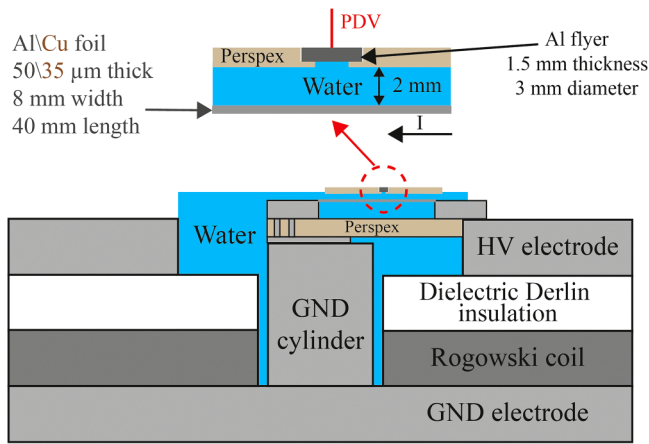


FIG. 6. Cross section of the experimental setup of the floating flyer configuration (lower diagram). The upper diagram is an enhanced view of the dashed red circle. The arrow marked by I denotes the direction of the current flow.

maximal amplitude of the current reached ~ 320 kA within ~ 340 ns, due to lower load inductance, estimated as ~ 32 nH, compared to the inductance of the floating target configuration. The energy density deposition rate was 2.54×10^5 and $1.17 \times 10^5 \frac{\text{MJ}}{\text{g s}}$ while the deposited energy density to the foils was $22 \text{ eV}/(\text{Al atom})$ and $24 \text{ eV}/(\text{Cu atom})$.

For each of the foils, the flyer temporal evolution of the velocity is presented in Fig. 11. An initial increase in velocity is visible, corresponding to the magnetic pressure exerted on the flyer, reaching almost the same values of ~ 70 m/s for both Al and Cu foils. Following this magnetic pushing, a strong shock generated by the exploding foils accelerates the flyer to velocities of ~ 800 m/s for both foils. This initial jump value, compared to the floating flyer configuration (Sec. II C), can be explained by the higher (~ 1.3 times) energy density deposition rate into the foil, resulting in increased shock velocity and, in turn, larger material flow velocity. For Cu foil explosions, a second jump in the velocity is clearly seen [Fig. 11(b)] associated with the expanding foil interacting with the flyer. For Al foil explosions, the second jump in velocity is not discernible from the PDV signal. For all three experiments with Al foil explosions, the second jump in velocity was not discernible from

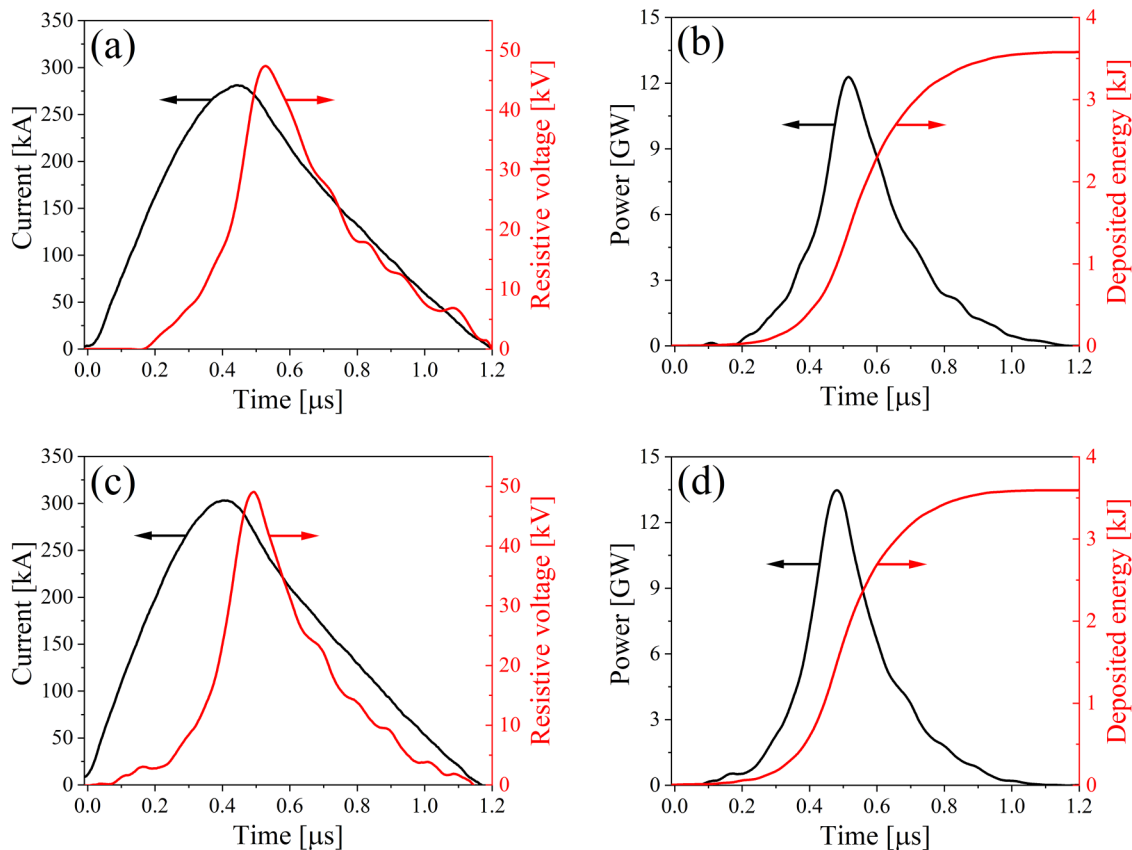


FIG. 7. Waveforms of the discharge current and resistive voltage [(a) and (c)], power, and deposited energy [(b) and (d)] for Al [(a) and (b)] and Cu [(c) and (d)] foils.

17 April 2024 11:03:13

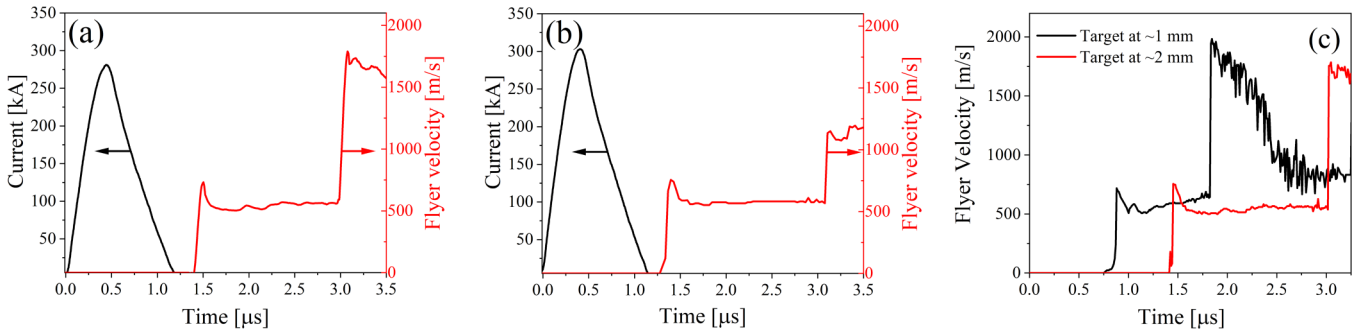


FIG. 8. Flyer velocity temporal evolution synchronized with the discharge current for Al (a) and Cu (b) foil explosions in floating flyer configuration with 2 mm foil–flyer gap and (c) for an exploding Al foil with the flyer situated a gap of 1 and 2 mm from the foil.

the PDV signal. At present, we do not have an explanation for this. We can only speculate that the absence of the second jump is the result of the smaller density of Al than that of Cu or/and that Al foil explosions are accompanied by much stronger radiation due to Al combustion,¹⁸ which can melt the Kapton. Thus, it is possible that this Kapton layer’s damping the Al foil–flyer interaction is significantly stronger than for Cu foil explosions. Nevertheless, one can see that the flyer velocity obtained in the first jump is ~2.5 times larger than for the strip-line configuration [see Fig. 4(b)], that is, a higher efficiency of the flyer acceleration by the hybrid exploding foil strip-line method.

Table I contains a summary of the maximal velocity obtained in each configuration. Additionally, the efficiency of the energy conversion from the stored energy into the load, the stored energy into the flyer kinetic energy, and the load energy conversion into the flyer kinetic energy are presented. We note that for foil explosions, the deposited energy into the foil is taken at times when the

power reaches its maximum value. For the strip-line configuration, the energy is taken as $E_{load} = 0.5LI^2$, where $L_{str} = 2.7$ nH is the strip-line inductance and $I \approx 450$ kA is the maximal amplitude of the discharge current. Also, the flyer area in the free flyer configuration was 5.4 times smaller than the area of the flyer in the strip-line configuration, which scales linearly with energy conversion into the flyer kinetic energy.¹⁰ Thus, in Table I, the energy conversion efficiencies for the free flyer obtained in the experiments were multiplied by the factor 5.4. The highest velocity and stored energy conversion efficiency into flyer kinetic energy was obtained for the free flyer but the highest load energy conversion efficiency was realized for the modified strip-line configuration.

III. DISCUSSION

Two-dimensional (2D) HD simulation using a self-developed code^{19,20} was performed to study the parameters of the exploding foil and waterflow parameters as well as the shock velocity. The simulation solves at each time step Euler’s equation in Lagrangian and energy,

$$\frac{\partial \rho}{\partial t} + \vec{\nabla} \cdot (\rho \vec{v}) = 0, \tag{1}$$

$$\frac{\partial \rho \vec{v}}{\partial t} + \vec{\nabla} (\rho \vec{v} \cdot \vec{v}) + \vec{\nabla} P = 0, \tag{2}$$

$$\frac{\partial \rho \epsilon}{\partial t} + \vec{\nabla} \cdot [(\rho \epsilon + P) \vec{v}] = 0. \tag{3}$$

Here, ρ , ϵ , \vec{v} , and P are the density, internal energy, velocity, and pressure, respectively. Equations (1)–(3) are coupled to the SESAME equations of state (EOS) tables for water, air, Al, and Cu so that $P = P(\rho, \epsilon)$ and $T = T(\rho, \epsilon)$. In the simulation, a triangular mesh is generated, recreating the experimental setup. The characteristic triangle size is of ~50 μm (the elements representing the Cu foil were set to ~35 μm), where each triangle is assigned with the corresponding material property. The vertices of each triangle are dislocated according to the sum of forces acting on its edge,

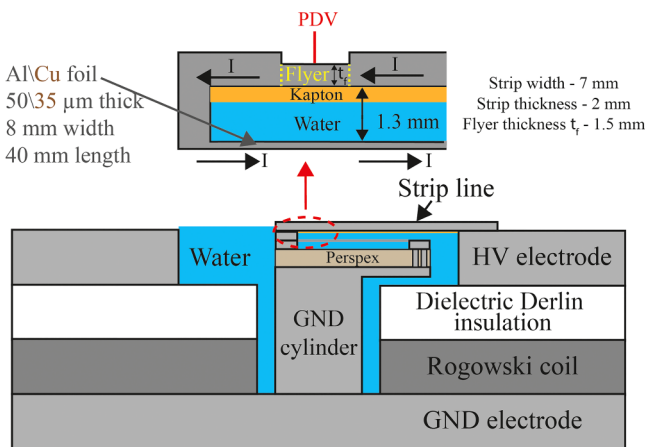


FIG. 9. Cross section of the experimental setup for the hybrid configuration (lower diagram). The upper diagram is an enhanced view of the dashed red circle. The arrows marked by I denote the direction of the current flow.

17 April 2024 11:03:13

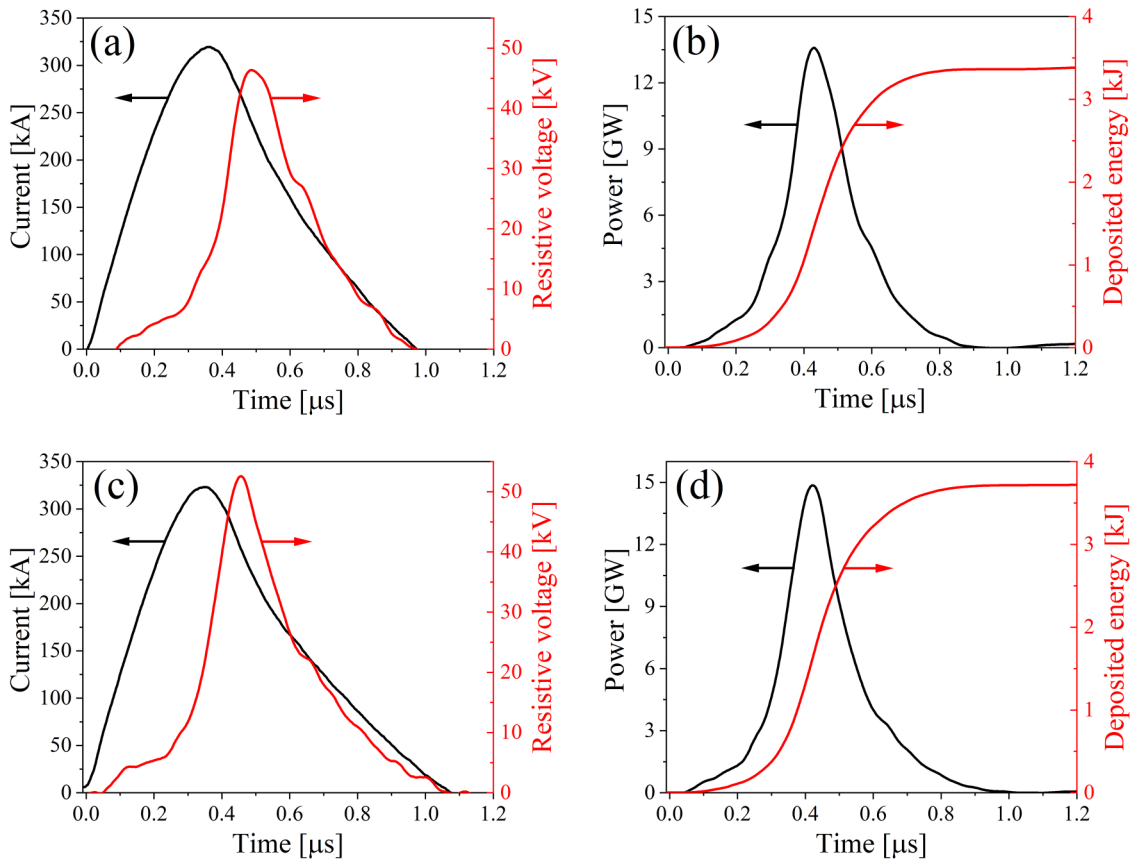


FIG. 10. Waveforms of the discharge current and resistive voltage [(a) and (c)], power, and deposited energy [(b) and (d)] for Al [(a) and (b)] and Cu [(c) and (d)] foils explosions.

17 April 2024 11:03:13

changing the area. The density and internal energy are then calculated, enabling the estimation of pressure and temperature according to the EOS tables. The input to the simulation is the experimentally measured deposited power. Since no optical

diagnostics of the shock front was available, the simulation is used to estimate the shock velocity before impacting the target. In the simulation, the shock front is defined to be 90% of the peak density behind the shock front. This simulated shock trajectory was fitted

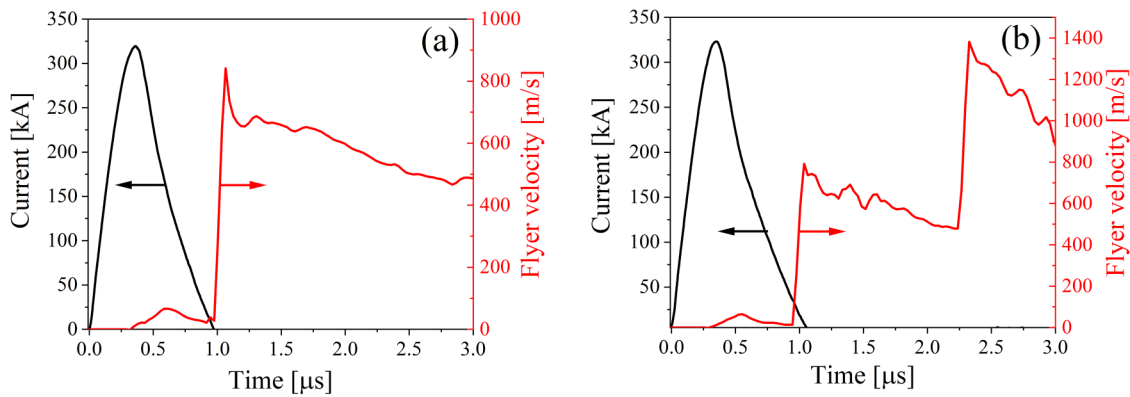


FIG. 11. Flyer velocity temporal evolution synchronized with the discharge current for Al (a) and Cu (b) foils in hybrid configuration.

TABLE I. Maximal velocity and energy conversion in all studied configurations.

	Maximal velocity (m/s)	Stored energy conversion into the load (%)	Stored energy conversion into flyer kinetic energy (%)	Load energy conversion into flyer kinetic energy (%)
Strip line	300	6	0.15	2.6
Modified strip line	1200	6	2.4	42
Exploding foil/ free flyer	2000	42 ^a	6.5	16.2
Hybrid strip-foil/exploding lower foil electrode	1400	42 ^a	3.7	7.8

^aDeposited energy considered at maximum power.

to a solution of the modified propagating blast wave²¹ of the form,

$$R(t) = a \cdot (t - b)^c, \quad (4)$$

where a , b , and c are fitting parameters. The shock velocity was calculated using the fitted Eq. (4). Results of the simulated and fitted trajectory, together with the shock velocity, are presented in Fig. 12 for Al and Cu foils.

The experimentally observed flyer velocity during the first jump, associated with the shock leaving the flyer and inducing material flow, was similar for both Al and Cu foils. The latter depends on the shock velocity inside the target, determined by the incoming shock velocity in water. Simulation results indicate that at the water–target interface, the velocity of the shock generated by the Al foil explosion was slightly (~5%) smaller than for Cu foil explosion. Here, we note that the simulations do not take into account Al combustion,²² which can add energy input into the shock, yielding a higher shock velocity. The simulated pressures and water density behind the shock front were $\sim 3 \times 10^9$ Pa and $\sim 1.33 \times 10^3$ kg/m³ for Al foil and $\sim 4 \times 10^9$ Pa and $\sim 1.4 \times 10^3$ kg/m³ for Cu foil.

Estimation of the flyer velocity, for the floating target configuration, given the shock generated by the exploding foil was

considered in previous research.²³ In the analytical model, described in detail in Ref. 23, the compression of a copper target by a water shock wave was analyzed, yielding a material velocity of a factor of two smaller than the flyer velocity at the free boundary. Solving the set of Eqs. (6)–(11) of Ref. 23, coupled with the Tait EOS,^{24,25} for copper and water, resulting in the waterflow velocity and pressure behind the shock front at the water-flyer boundary presented in Fig. 13(a). The dependence of the flyer velocity and the corresponding pressure in the aluminum flyer on the incoming shock velocity is presented in Fig. 13(b).

For the given experimental conditions, combined with results from the 2D HD simulations, we can estimate that for a shock impacting the target with velocities of ~ 3500 m/s, the corresponding material flow velocity and pressure reach ~ 1000 m/s and ~ 8 GPa. Here, we note that this model does not account for shock attenuation in the target, which in our case was of ~ 1.5 mm, meaning that this result is an overestimation. Nevertheless, this simplified analytical model yields values that are close to those obtained in experiments.

Given our experimental results with ~ 2000 m/s Al flyers hitting an Al target, 18 GPa pressure will be realized for $D = 5.38 + 1.35U_p$ (units are in km/s)²⁵ generating a shock velocity of 6730 m/s, where D is the shock velocity and U_p is the particle

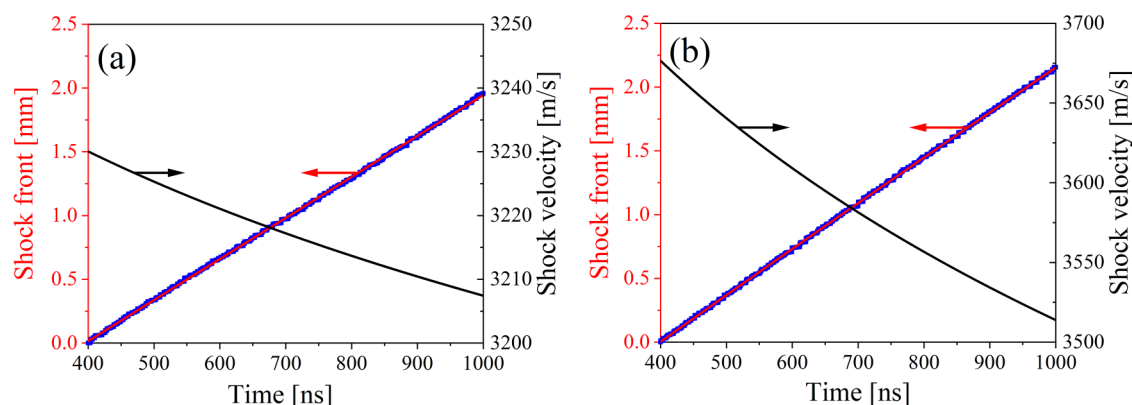


FIG. 12. Simulated shock trajectory (blue), fitted trajectory (red), and shock velocity (black) for Al (a) and Cu (b) foils. $t = 0$ is the time at the maximum of the deposited power.

17 April 2024 11:03:13

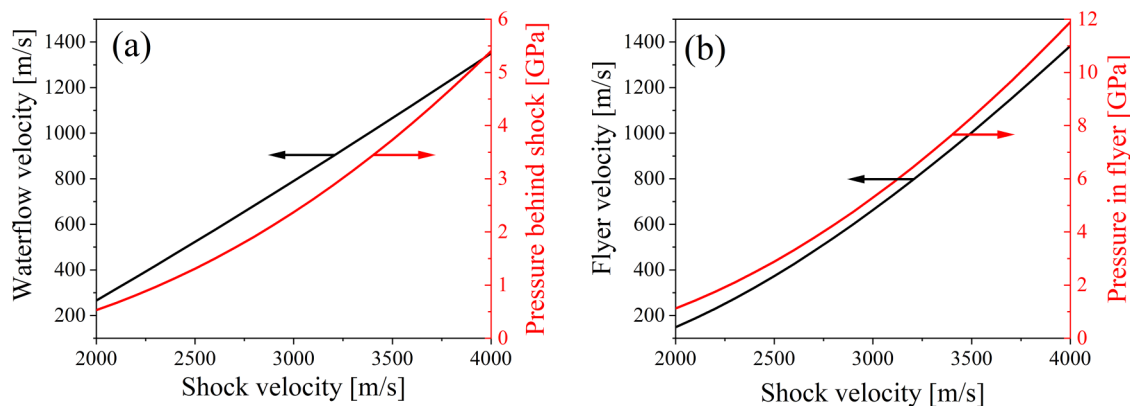


FIG. 13. Waterflow velocity and water pressure behind the shock front (a) and flyer velocity with corresponding pressure (b) plotted against incoming shock velocity. $t = 0$ is the time at the maximum of the deposited power.

velocity of the flyer. Increasing the incoming shock velocity to 6000 m/s can result in 2000 m/s particle velocity, yielding higher pressure in an Al target upon flyer impact, realizing pressures of over 40 GPa.

IV. SUMMARY

We have presented several methods for flyer acceleration, utilizing water both as an insulator and as a medium, which transfers kinetic energy from the exploding foil to accelerated flyers. We demonstrated that a simple change in the geometry of the strip-line configuration can significantly increase magnetic pushing, resulting in higher flyer velocity. The acceleration of flyers using underwater explosions of Al and Cu foils was demonstrated, producing sharp rises in velocity with the addition of a second flyer velocity jump, possibly caused by the expansion of the foil. A design of a hybrid configuration was suggested in which both effects of the strip line and the exploding foil are combined. Thus, this approach can be considered to be useful for studies of high stress material properties^{26,27} and as a useful tool for probing the Richtmyer–Meshkov instability similar to that demonstrated in recent research.²⁸ Finally, with more powerful pulse generators, which would allow larger energy density deposition rates on the $\sim 10^{-7}$ s timescale, significantly stronger shock waves would be generated in water leading to higher flyer velocities than those realized in the present research.

ACKNOWLEDGMENTS

We are grateful to Dr. J. Leopold for fruitful discussions. This research was supported by the Israel Science Foundation (Grant No. 418/22).

AUTHOR DECLARATIONS

Conflict of Interest

The authors have no conflicts to disclose.

Author Contributions

D. Maler: Conceptualization (equal); Data curation (equal); Formal analysis (equal); Methodology (equal); Software (equal); Writing – original draft (equal); Writing – review & editing (equal). **G. Liziakin:** Formal analysis (equal); Software (equal); Writing – original draft (equal). **O. Belozarov:** Data curation (equal); Methodology (equal). **S. Efimov:** Data curation (equal); Formal analysis (equal); Methodology (equal); Supervision (supporting). **D. Rakhmievich:** Conceptualization (equal); Data curation (equal); Formal analysis (equal); Methodology (equal); Writing – original draft (equal). **K. Cohen:** Conceptualization (equal); Supervision (equal); Writing – original draft (equal). **Ya. E. Krasik:** Conceptualization (equal); Methodology (equal); Supervision (lead); Writing – original draft (equal).

DATA AVAILABILITY

The data that support the findings of this study are available from the corresponding author upon request.

REFERENCES

- M. D. Knudson, R. W. Lemke, D. B. Hayes, C. A. Hall, C. Deeney, and J. R. Asay, *J. Appl. Phys.* **94**, 4420 (2003).
- M. D. Knudson, D. L. Hanson, J. E. Bailey, C. A. Hall, J. R. Asay, and C. Deeney, *Phys. Rev. B* **69**, 1 (2004).
- H. Nagao, K. G. Nakamura, K. Kondo, N. Ozaki, K. Takamatsu, T. Ono, T. Shiota, D. Ichinose, K. A. Tanaka, K. Wakabayashi, K. Okada, M. Yoshida, M. Nakai, K. Nagai, K. Shigemori, T. Sakaiya, and K. Otani, *Phys. Plasmas* **13**, 052705 (2006).
- A. Bushman, I. Lomonosov, V. Fortov, K. Khishchenko, M. Zhernokletov, and Y. Sutulov, *Sov. J. Exp. Theor. Phys.* **82**, 895 (1996).
- L. C. Chhabildas, L. M. Barker, J. R. Asay, T. G. Trucano, G. I. Kerley, and J. E. Dunn, “Launch capabilities to over 10 km/s,” in *Shock Compression of Condensed Matter—1991* (Elsevier, 1992), pp. 1025–1031.
- H. Shu, X. Huang, J. Ye, G. Jia, J. Wu, and S. Fu, *Laser Part. Beams* **35**, 145 (2017).
- S. Stekovic, H. K. Springer, M. Bhowmick, D. D. Dlott, and D. S. Stewart, *J. Appl. Phys.* **129**, 195901 (2021).

17 April 2024 11:03:13

- ⁸T. Ao, J. R. Asay, S. Chantrenne, M. R. Baer, and C. A. Hall, *Rev. Sci. Instrum.* **79**, 013903 (2008).
- ⁹D. Maler, A. Rososhek, S. Efimov, A. Virozub, and Y. E. Krasik, *J. Appl. Phys.* **129**, 034901 (2021).
- ¹⁰D. Maler, S. Efimov, and Y. E. Krasik, *J. Appl. Phys.* **131**, 074902 (2022).
- ¹¹N. Bennett, D. R. Welch, K. Cochrane, K. Leung, C. Thoma, M. E. Cuneo, and G. Frye-Mason, *Phys. Rev. Accel. Beams* **26**, 40401 (2023).
- ¹²S. A. Chaikovskiy, V. I. Oreshkin, G. A. Mesyats, N. A. Ratakhin, I. M. Datsko, and B. A. Kablambaev, *Phys. Plasmas* **16**, 042701 (2009).
- ¹³A. Rososhek, S. Efimov, A. Virozub, D. Maler, and Y. E. Krasik, *Appl. Phys. Lett.* **115**, 074101 (2019).
- ¹⁴J. E. Osher, G. Barnes, H. H. Chau, R. S. Lee, C. Lee, R. Speer, and R. C. Weingart, *IEEE Trans. Plasma Sci.* **17**, 392 (1989).
- ¹⁵J. Osher, R. Gathers, H. Chau, R. Lee, G. Pomykal, and R. Weingart, *Int. J. Impact Eng.* **10**, 439 (1990).
- ¹⁶B. M. Kovalchuk, A. V. Kharlov, V. B. Zorin, and A. A. Zherlitsyn, *Rev. Sci. Instrum.* **80**, 083504 (2009).
- ¹⁷T. Ao and D. H. Dolan, "SIRHEN: A data reduction program for photonic Doppler velocimetry measurements," SAND2010-3628, 2010.
- ¹⁸N. Asmedyanov, R. Grikshtas, D. Maler, G. Liziakin, and Ya. E. Krasik, "Underwater microsecond timescale electrical explosions of aluminum and copper foils," *J. Appl. Phys.* **134**, 165902 (2023).
- ¹⁹D. Maler, S. Efimov, M. Liverts, S. Theocharous, J. Strucka, Y. Yao, W. Proud, A. Rack, B. Lukic, S. N. Bland, and Y. E. Krasik, *Phys. Plasmas* **29**, 063502 (2022).
- ²⁰D. Maler, R. Grikshtas, S. Efimov, L. Merzlikin, M. Liverts, M. Kozlov, and Y. E. Krasik, *Phys. Plasmas* **30**, 022710 (2023).
- ²¹C. Clarke and B. Carswell, *Principles of Astrophysical Fluid Dynamics* (Cambridge University Press, 2007).
- ²²A. Rososhek, S. Efimov, A. Goldman, S. V. Tewari, and Y. E. Krasik, *Phys. Plasmas* **26**, 053510 (2019).
- ²³V. Gurovich, A. Virozub, A. Rososhek, S. Bland, R. B. Spielman, and Y. E. Krasik, *J. Appl. Phys.* **123**, 185902 (2018).
- ²⁴J. R. MacDonald, *Rev. Mod. Phys.* **38**, 669 (1966).
- ²⁵M. van Thiel, "Compendium of shock wave data," Lawrence Livermore Laboratory Report UCRL-50108, 1977, p. 76.
- ²⁶V. E. Fortov, R. F. Trunin, L. V. Al'tshuler, and A. I. Funtikov, *High-Pressure Shock Compression of Solids VII: Shock Waves and Extreme States of Matter* (Springer-Verlag, New York, 2004).
- ²⁷C. A. McCoy, M. D. Knudson, and M. P. Desjarlais, *Phys. Rev. B* **100**, 054107 (2019).
- ²⁸J. Strucka, B. Lukic, M. Koerner, J. W. D. Halliday, Y. Yao, K. Mughal, D. Maler, S. Efimov, J. Skidmore, A. Rack, Y. E. Krasik, J. Chittenden, and S. N. Bland, *Phys. Fluids* **35**, 044108 (2023).